Exact Regions of Superradiant Instability of Kerr-Newman Black Holes and Massive Scalar Fields

John Adrian B. Baybay and Kevin T. Grosvenor

National Institute of Physics, University of the Philippines Diliman, Quezon City 1101, Philippines

E-mail: jbaybay@nip.upd.edu.ph, kgrosvenor@nip.upd.edu.ph

ABSTRACT: We investigate the superradiant instability of Kerr–Newman black holes in the presence of a massive, charged scalar field using the Vieira–Bezerra–Kokkotas (VBK) method. We study the solutions of the exact polynomial condition for quasibound state frequencies and determine the domain of superradiant instability in parameter space without relying on the hydrogenic approximation or numerics. We derive the minimum scalar mass needed for quasibound states to exist, and identify the precise overlap region between the quasibound and superradiant conditions where instability can occur. Through a perturbative analysis of the resonance equation, we obtain analytic expressions for the instability boundaries and growth rates, and clarify their relation to previous numerical results. Our analysis reveals how the instability region shifts from nearly neutral Kerr black holes for light fields to highly charged near-extremal Kerr–Newman black holes for heavier fields, while remaining absent in the Reissner–Nordström limit.

^{*}The authors are ordered purely alphabetically and should all be viewed as the co-first authors.

C	ontents	
1.	Introduction	1
2.	Klein-Gordon Field in the Kerr-Newman Background	3
3.	The VBK method vs. the Hydrogenic Approximation	4
4.	The Regions of Superradiant Instability	6
	4.1. Quasibound States	7
	4.2. Perturbative Analysis of the Quasibound State Condition	7
	4.3. Superradiant Modes	9
5.	Scalar Field Growth Rate	11
	5.1. The Analytics vs. Numerics Discrepancy	12
6.	Conclusion and Outlook	14

1. Introduction

Since black holes are immersed in an environment, it is of great interest to investigate the effects on the black hole of its interaction with that environment (e.g. for gravitational wave searches [1, 2], for the study of active galactic nuclei [3], for black hole imaging [4], jets [5], and for dark matter searches [6–8]). These effects can present themselves as perturbations that may grow in time and eventually lead to the instability of the black hole. An example of such an instability is black hole superradiance. The effect of superradiance, as introduced by Dicke [9], is a radiation enhancement process that can arise in systems with dissipation. This phenomenon can be observed in many different systems of interest in physics such as in optics, in quantum mechanics, in condensed matter systems, and especially in black holes (see [10] for a general review of superradiance as well as applications to different physical systems; see also [11–14] for various specific applications).

Black hole superradiance occurs when an incident field extracts energy away from the black hole resulting in an amplified scattered field. This can happen for modes with frequency ω below a certain critical frequency ω_c , which depends on the spin and charge of the black hole. This effect can be further amplified by surrounding the black hole with hypothetical reflecting mirrors, thereby trapping the amplified field in the vicinity of the black hole and forcing it to undergo the superradiant process repeatedly. For as long as the superradiant condition is satisfied, the external field continues to extract energy from the black hole and its total energy grows exponentially until immense radiation pressure destroys the mirrors. This

is known in the literature as a black hole superradiant instability, or a black hole bomb [15]. Though highly evocative, the hypothetical mirror setup is not, in fact, necessary to induce an instability of the black hole; one simply needs to consider massive fields to achieve the same effect. When the field has a mass μ such that $\mu > \omega$, the mass effectively acts as the reflecting mirror [16], creating a cloud around the black hole. This is called a gravitational atom, as in a certain limit it behaves essentially analogously to the hydrogen atom [17–22]. This phenomenon works for massive bosons and not for fermions due to the Pauli exclusion principle [23]. The approximations leading to the gravitational atom picture were first systematized by Starobinski [24], and later by Detweiler [25], to solve the Klein-Gordon equation in a black hole background. It was then further posited that black holes can act as particle detectors which can be used as probes to detect new physics. One particular example of new physics one can hope to detect with the help of gravitational waves associated with black hole superradiant instability is the existence of ultralight bosons [26]. Recent further developments include studies on the effects of gravitational atoms in binary systems [27].

In 2016, Vieira and Bezerra presented a new method to find exact solutions of the Klein-Gordon equation in different black-hole background spacetimes, including the Kerr-Newman black hole [28]. In 2021, Vieira and Kokkotas applied the same technique to study Schwarzschild acoustic black holes [28]. This was followed by a study of the superradiant instability of Kerr-Newman black holes in the presence of a massive scalar field using this method, which they then coined the Vieira–Bezerra–Kokkotas (VBK) method [29]. This method uses polynomial conditions of the Heun function to solve for resonant modes that form quasibound states around the black hole. The core result of [29] is to furnish a quartic equation, called the characteristic equation, for the resonant frequencies of the scalar field modes. The solutions to this quartic equation were plotted and to check for instabilities, the authors looked at the conditions under which the solution grows over time, that is, $\operatorname{Im} \omega > 0$, where ω is the mode frequency.

In this paper, we will use the VBK method presented in [29] to completely specify the regions of black hole superradiant instability as a function of the parameters of the black hole (spin a and charge Q) and the surrounding scalar field (mass μ). There are plenty of studies of black hole superradiant instability for the Kerr black hole [16, 30, 31]. The majority of these studies work in the limit of a very light external scalar field with a mass parameter μ satisfying $\mu M \ll 1$, where M is the mass of the black hole. There are likely at least three reasons for this: 1. The ligher the field is, the broader is the range of a over which superradiant instability can occur; 2. The smaller the value of a, the smaller the value of μ needed for superradiant instability; and 3. Most phenomenological models take the scalar field to be the QCD axion [32–35], which is constrained to be extremely light. As such, there does not appear to be in the literature a complete and systematic characterization of the region of superradiant instability in the parameter space spanned by the spin a and charge a0 of the Kerr-Newman black hole and the mass a1 and charge a2 of the scalar field. The goal of this paper is to fill in this gap.

We will furnish a plot, in fig. 4b that shows the region of the space of Kerr-Newman

black holes that are unstable to superradiance given the mass of the external scalar field. Compare this, for example, with [36], which describes conditions for superradiant instability of Kerr-Newman black holes due to a charged massive scalar field in terms of the existence of a "trapping" effective potential, though, in truth, derives explicit results only in the Kerr (Q=0) limit. The VBK method allows us to exactly characterize the regions of black-hole parameter space that are unstable to superradiance without the need for an intervening analysis of the effective potential by working directly with the modes of the scalar field themselves. This problem serves as an excellent testing ground for this method and provides a good opportunity to compare it with the methods of hydrogenic approximation and numerics.

The presentation of the paper will proceed as follows. In section 2, we will introduce the Klein-Gordon equation in the Kerr-Newman background. In section 3 and give a quick overview of the VBK method as well as the standard hydrogenic approximation. In section 4, we will then show how to solve for the quasibound states and superradiant states and plot their respective regions in the parameter space. We take the overlap of these two regions to determine the region of instability. In section 5, we fix a and Q, instead tuning q to determine the region where the scalar field mode grows over time and compare with the numerical results of Furuhashi and Nambu [37]. We highlight the discrepancies between the numerical results and our exact analytical results and identify the origin of these discrepancies. Finally, we conclude with some discussions and future directions. Throughout this paper, we use the reduced units $G = \hbar = c = 1$.

2. Klein-Gordon Field in the Kerr-Newman Background

A stationary axisymmetric charged rotating black hole may be modeled using the Kerr Newman metric [38]. In the Boyer-Lindquist coordinates, the line element is written as

$$ds^{2} = -\frac{\Delta}{\rho^{2}}(dt - a\sin^{2}\theta d\phi)^{2} + \frac{\sin^{2}\theta}{\rho^{2}}\left[(r^{2} + a^{2})d\phi - adt\right]^{2} + \frac{\rho^{2}}{\Delta}dr^{2} + \rho^{2}d\theta^{2},\tag{2.1}$$

where

$$\Delta = r^2 + a^2 - 2Mr + Q^2,$$
 $\rho^2 = r^2 + a^2 \cos^2 \theta,$ (2.2)

with M being the mass of the black hole, a its spin, and Q its charge. The limit a=0 corresponds to the Reissner-Nordström (RN) black hole, the limit Q=0 corresponds to the Kerr black hole, and the limit a=Q=0 corresponds to the Schwarzschild black hole. The KN metric has a physical singularity at $\rho=0$. There are also coordinate singularities at the roots of the equation $\Delta=0$, which are

$$r_{\pm} = M \pm \sqrt{M^2 - a^2 - Q^2}. (2.3)$$

Thus, we can write

$$\Delta(r) = (r - r_{+})(r - r_{-}). \tag{2.4}$$

The surface $r = r_{+}$ is called the outer horizon and $r = r_{-}$ the inner horizon. Lastly, the KN spacetime is endowed with a Maxwell potential given by

$$A_{\mu} = \frac{Qr}{\rho^2} (1, 0, 0, -a \sin^2 \theta). \tag{2.5}$$

The equation of motion that describes a scalar field Ψ , with mass μ and charge q, propagating in a curved spacetime and in the presence of an electromagnetic field, is given by

$$\left[\frac{1}{\sqrt{-g}}\partial_{\mu}\left(g^{\mu\nu}\sqrt{-g}\,\partial_{\nu}\right) + iq\left(\partial_{\mu}A^{\mu}\right) + 2iqA^{\mu}\partial_{\mu} + \frac{iq}{\sqrt{-g}}A^{\mu}\left(\partial_{\mu}\sqrt{-g}\right) - q^{2}A^{\mu}A_{\mu} + \mu^{2}\right]\Psi = 0,$$
(2.6)

where $g = \det(g_{\mu\nu})$. We assume a separable solution

$$\Psi(t, r, \theta, \phi) = e^{-i\omega t} R(r) P(\theta) e^{im\phi}, \qquad (2.7)$$

with R(r) as the radial function, $P(\theta)$ as the angular function, and m being the magnetic quantum number. Using the ansatz (2.7), we find that eq. (2.6) separates into two ordinary differential equations given by

$$\frac{1}{\sin\theta} \frac{d}{d\theta} \left[\sin\theta \frac{dP(\theta)}{d\theta} \right] + \left[\lambda + a^2(\mu^2 - \omega^2) \sin^2\theta - \frac{m^2}{\sin^2\theta} \right] P(\theta) = 0, \tag{2.8}$$

and

$$\frac{d}{dr} \left[\Delta(r) \frac{dR(r)}{dr} \right] + \left\{ \frac{[\omega(r^2 + a^2) - am - qQr]^2}{\Delta(r)} - [\lambda + \mu^2(r^2 + a^2) - 2am\omega] \right\} R(r) = 0, (2.9)$$

where λ is a separation constant. From here it is standard to use numerical techniques to solve this pair of differential equations. However, Starobinskii [24] showed that the equations can be solved analytically in the limit $\omega M \ll 1$ and $\mu M \ll 1$. Additionally, in the region $r \gg M$, the equations reduce to those of the hydrogen atom, with $\lambda \approx \ell(\ell+1)$ and ℓ being the azimuthal quantum number [25]. Recently, however, Viera, Bezerra, and Muniz [29] used the VBK method to find exact solutions of equation (2.6) involving the confluent Heun functions. For our purposes, the main result of this method is an exact equation for the resonance frequency modes of the charged scalar field in a Kerr-Newman black hole background, given in eq. (3.9). This can then be used to determine the conditions under which black hole superradiant instability will take place:

- The formation of bound states around the black hole requires $\text{Re}\left[\sqrt{\mu^2-\omega^2}\right]>0$; and
- The superradiant condition $\omega < \omega_c$ must be satisfied.

3. The VBK method vs. the Hydrogenic Approximation

To determine quasibound states in the hydrogenic approximation we consider scalar fields that are light enough such that their Compton wavelength is much larger than that of the black hole. That is, defining $\alpha = \mu M$, which can be thought of as gravitational fine structure constant [17], this limit is $\alpha \ll 1$. In this limit, the Klein-Gordon equation for a scalar field in the Kerr black hole background (we set Q = 0 for now for simplicity) takes the form of a Schroedinger equation, written as

$$i\frac{\partial\Psi}{\partial t} = -\frac{1}{2\mu}\nabla^2\Psi + V_{\text{eff}}(r)\Psi, \tag{3.1}$$

where the effective potential is

$$V_{\text{eff}} = -\frac{\alpha}{r} + \frac{\ell(\ell+1)}{2\mu r^2}.$$
(3.2)

The form of equation (3.1) is reminiscent of the Hydrogen atom and allows us to solve for the spectrum by analogy [25]:

$$E_n = -\frac{\alpha^2 \mu}{2n^2},$$
 $\operatorname{Re} \omega_n = \mu + E_n = \mu \left(1 - \frac{\alpha^2}{2n^2}\right).$ (3.3)

The radial extent of the scalar field cloud is determined in a way analogous to the Bohr radius and orbital radii of hydrogen. The growth rate of the cloud is determined by the imaginary part of the frequency.

In contrast, the VBK method proceeds without approximations. The radial equation (2.9), may be written as

$$\frac{d^{2}R}{dr^{2}} + \left(\frac{1}{r - r_{+}} + \frac{1}{r - r_{-}}\right) \frac{dR}{dr} + \left(\frac{\left[\omega\left(r^{2} + a^{2}\right) - am - eQr\right]^{2}}{(r - r_{+})^{2}(r - r_{-})^{2}} - \frac{\lambda + \mu^{2}\left(r^{2} + a^{2}\right) - 2am\omega}{(r - r_{+})(r - r_{-})}\right) R = 0.$$
(3.4)

This form of the radial equation indicates that there are two finite regular singularities associated with the two event horizons, i.e. r_+ and r_- , and an irregular singularity at infinity. Thus, we can perform the Möbius transformation

$$x = \frac{r - r_{-}}{r_{+} - r_{-}} \tag{3.5}$$

to move the regular singularity at $r = r_{-}$ to x = 0, the one at $r = r_{+}$ to x = 1, and the irregular singularity at $r = \infty$ to $x = \infty$. The homotopic transformation

$$R(r) = x^{D_0}(x-1)^{D_1}e^{D_2x}U(x), (3.6)$$

where the constants D_i are given by

$$D_0 = -i\frac{\omega(r_-^2 + a^2) - am - qQr_-}{r_+ - r_-},$$
(3.7a)

$$D_1 = -i\frac{\omega(r_+^2 + a^2) - am - qQr_+}{r_+ - r_-},$$
(3.7b)

$$D_2 = -(r_+ - r_-)\sqrt{\mu^2 - \omega^2},\tag{3.7c}$$

turns the radial equation into the confluent Heun equation

$$\frac{d^2U}{dx^2} + \left(2D_2 + \frac{1+2D_0}{x} + \frac{1+2D_1}{x-1}\right)\frac{dU}{dx} + \left(\frac{\xi}{x} + \frac{\zeta}{x-1}\right)U = 0,\tag{3.8}$$

where ξ and ζ are complicated expressions in terms of the parameters a, Q, μ, q, M, m , and ω . The confluent Heun functions of first and second kind furnish solutions with potentially different linear combinations of these two solutions being appropriate to describe the solution in a neighborhood of each of the three singularities. These solutions must be made to match along the intersection of their domains. The result is a polynomial condition similar in principle to the one that derives from the "halting" problem of the expansions involved in the Frobenius method (e.g., that the wave functions of the 1d quantum harmonic oscillator must take the form of a finite-degree polynomial multiplying a Gaussian – the Hermite functions). There is just the added complication here of having multiple overlapping expansions, one around each singularity, but the procedure is otherwise analogous. The degree of the polynomial that we must force the confluent Heun functions to become is called the overtone number, N, which must thus be a non-negative integer. Much in the same way that the halting problem in the Frobenius method determines the spectrum (e.g., by expressing the harmonic oscillator energy in terms of the quantum number n, which is the finite degree of the associated Hermite polynomial), the VBK method furnishes an exact equation for the resonance frequencies ω of the modes of the scalar field in terms of the overtone number N, the black hole parameters a, Q, and M, and the scalar field parameters μ and q:

$$\frac{qQ\omega + M(\mu^2 - 2\omega^2)}{\sqrt{\mu^2 - \omega^2}} + N + 1 + i\frac{am + qQM + (Q^2 - 2M^2)\omega}{\sqrt{M^2 - a^2 - Q^2}} = 0.$$
 (3.9)

This can be massaged into a quartic equation for ω . Therefore, there are generally four solutions and, in principle, there is a closed-form formula for these involving only arithmetic operations and roots. However, this formula is complicated and cumbersome to use and when applying any approximations or limits, it is generally simpler and more transparent to apply them to the equation first rather than directly on the solutions themselves. Furthermore, we are only interested in the solution that satisfies $\omega \approx \mu$, but which one that is out of the four solutions changes depending on the various parameters due to branch ambiguities in the definitions of the root operations. This problem is well documented in [29]. We now proceed to describe how we will use and analyze this equation.

4. The Regions of Superradiant Instability

We will now examine the conditions that must be satisfied in order for the black hole to develop a superradiant instability. We require that there be both quasibound states and superradiant modes. The existence of quasibound states allows the formation of scalar field clouds surrounding the black hole that can continuously extract energy from the black hole via superradiant scattering.

4.1. Quasibound States

To determine if there are quasibound state modes, we must first solve the radial equation and then impose the boundary conditions

- (i) The radial solution should describe an incoming wave at the exterior event horizon;
- (ii) The radial solution must tend to zero far from the black hole at asymptotic infinity.

Let R_1 denote the expansion of the the radial function near $r = r_+$. The first condition is satisfied by setting the solution to be

$$R_1(r) \sim C_1(r - r_+)e^{-\frac{i}{2\kappa_+}(\omega - \omega_c)},$$
 (4.1)

where C_1 is a constant,

$$\kappa_{+} = \frac{r_{+} - r_{-}}{2(r_{+}^{2} + a^{2})},\tag{4.2}$$

and the critical frequency is given by

$$\omega_c = m\Omega_+ + q\Phi_+, \qquad \qquad \Omega_+ = \frac{a}{r_+^2 + a^2}, \qquad \qquad \Phi_+ = \frac{Qr_+}{r_+^2 + a^2}. \tag{4.3}$$

Let R_{∞} be the asymptotic form of the solution as $r \to \infty$. Then, we find

$$R_{\infty}(r) \sim C_{\infty} r^{-(1+p)} e^{-\gamma r},\tag{4.4}$$

where

$$p = \frac{qQ\omega + M(\mu^2 - 2\omega^2)}{\gamma} \quad \text{and} \quad \gamma = \sqrt{\mu^2 - \omega^2}.$$
 (4.5)

The asymptotic boundary condition requires that

$$\operatorname{Re}\left[\sqrt{\mu^2 - \omega^2}\right] > 0. \tag{4.6}$$

Therefore, $\omega = \mu$ at the boundary of the quasibound-state region.

4.2. Perturbative Analysis of the Quasibound State Condition

We may write the resonance equation in the form

$$\left(\overline{N}D + i\left[am + M(qQ - \mu M) - (M^2 - Q^2)\mu + (2M^2 - Q^2)(\mu - \omega)\right]\right)^2(\mu^2 - \omega^2)
= D^2\left((qQ - \mu M)\mu - qQ(\mu - \omega) + 2M(\mu^2 - \omega^2)\right)^2,$$
(4.7)

where

$$\overline{N} = N + 1,$$
 $D = \sqrt{M^2 - a^2 - Q^2}.$ (4.8)

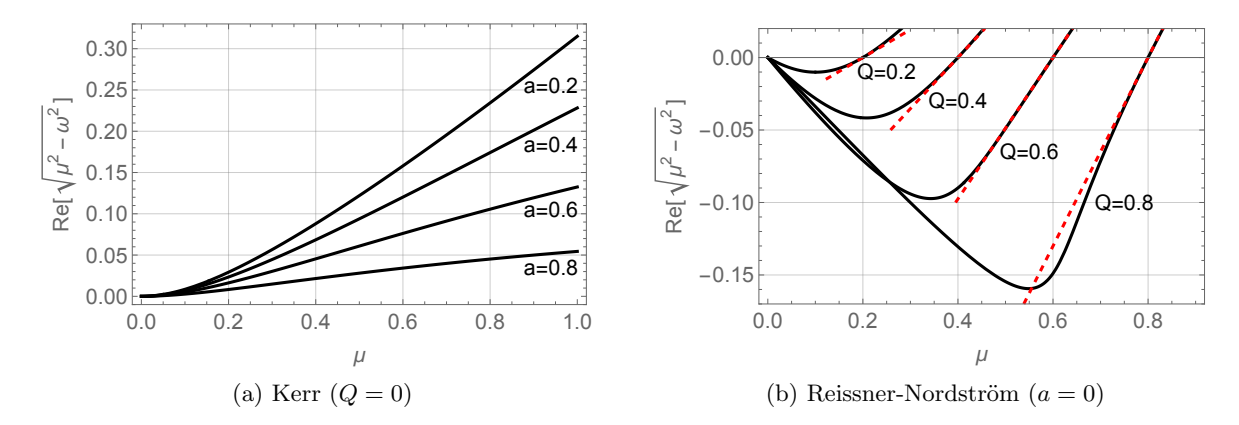


Figure 1: Plots of Re $\left[\sqrt{\mu^2 - \omega^2}\right]$ versus μ for (a) Kerr with various different values of a and (b) Reissner-Nordström with various different values of Q. For Kerr, the plots vanish exactly at $\mu = 0$ and are flat, as predicted by (4.11) since $\mu_0 = qQ/M = 0$ for Kerr. In addition to vanishing at $\mu = 0$, the plots for RN have another root at $\mu = \mu_0 = qQ/M$. The linear approximation (4.11) is plotted as red dashed lines for each value of Q.

If we set $\omega = \mu$, then, the equation reduces to

$$D^{2}\mu^{2}(qQ - M\mu)^{2} = 0, (4.9)$$

the solution to which is

$$\mu = \mu_0 \equiv \frac{qQ}{M}.\tag{4.10}$$

We expand (4.7) around $\mu = \mu_0$ and solve for ω to lowest order in $\mu - \mu_0$, giving the result

$$\operatorname{Re}\left[\sqrt{\mu^2 - \omega^2}\right] = \left(\frac{\overline{N}D^2 \mu_0 M}{(\overline{N}D)^2 + [am + \mu_0(Q^2 - M^2)]^2}\right) (\mu - \mu_0), \tag{4.11}$$

Note that $\operatorname{Re}\left[\sqrt{\mu^2 - \omega^2}\right]$ is positive for $\mu > \mu_0$ and negative for $\mu < \mu_0$. This is perfectly clear in the plots of this quantity in figs. 1b and 2; this analysis demonstrates that this is true at least in the vicinity of $\mu = \mu_0$, but the plots show that this remains true well beyond this point up to and even beyond the $\mu M = 1$ threshold. Therefore, there are no quasibound states when $\mu < \mu_0$ and there are quasibound states when $\mu > \mu_0$.

For Kerr shown in fig. 1a, we have $\mu_0 = 0$ and so the plots vanish only at $\mu = 0$ and the linear approximation (4.11) vanishes as well, which is consistent with the fact that the plots are flat at $\mu = 0$. Meanwhile, for Reissner-Nordström, in addition to the trivial root at $\mu = 0$, the plots have a nonzero root at $\mu = \mu_0 = qQ/M$. At that point, the linear approximation (4.11) is plotted as the red dashed lines in fig. 1b and, indeed, faithfully reproduce the plot near the root. In fig 2 is plotted Re $\left[\sqrt{\mu^2 - \omega^2}\right]$ versus μ for Kerr-Newman black hole backgrounds with various different values of a and a0. Again, the plots are negative for a1 and positive for a2 and eq. (4.11), plotted as red dashed lines, gives good approximations near a4 and a5.

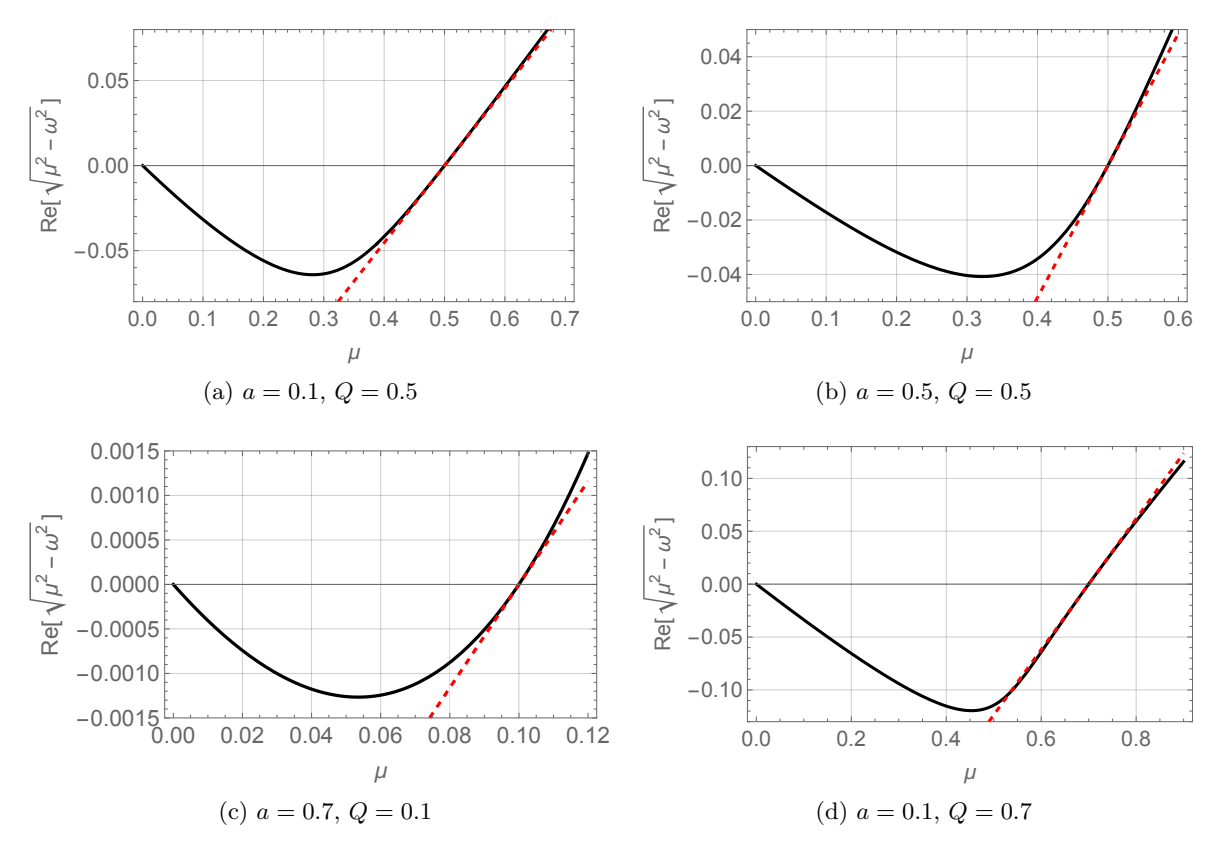


Figure 2: Plots of Re $\left[\sqrt{\mu^2 - \omega^2}\right]$ versus μ for different values of the Kerr-Newman black hole parameters a and Q. The red dashed line is the linear approximation (4.11).

4.3. Superradiant Modes

The critical frequency ω_c below which superradiance occurs is [9],

$$\omega < \omega_c = \frac{ma + qQr_+}{r_+^2 + a^2}. (4.12)$$

Since $\omega \lesssim \mu$, we can approximate the condition that μ must satisfy to allow for superradiance to be

$$\mu < \omega_c = \frac{ma + qQr_+}{r_+^2 + a^2}. (4.13)$$

We plot this region for Kerr in fig. 3a, for Reissner-Nordström in fig. 3b, and for the Kerr-Newman black hole with μ vs. a for various values of Q in fig. 3c and μ vs. Q for various values of a in fig. 3d.

It is particularly instructive to plot the regions of superradiance in the plane of black hole parameters a and Q for various different values of the scalar field mass parameter μ . Furthermore, we can superpose on this the region where there are quasibound states. For these plots, we set M=1, m=1, and q=1. Thus, the quasibound state region is simply the

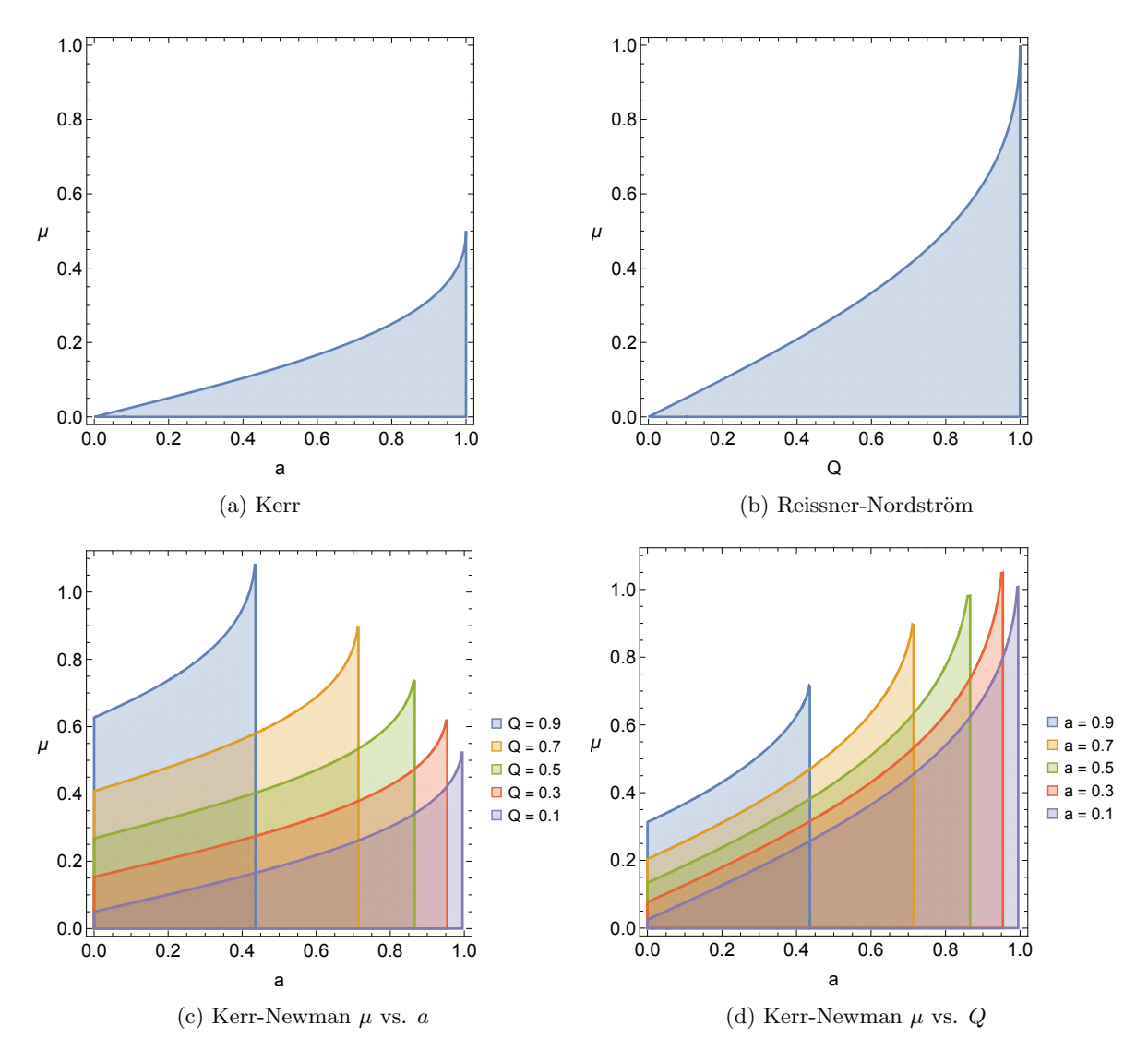
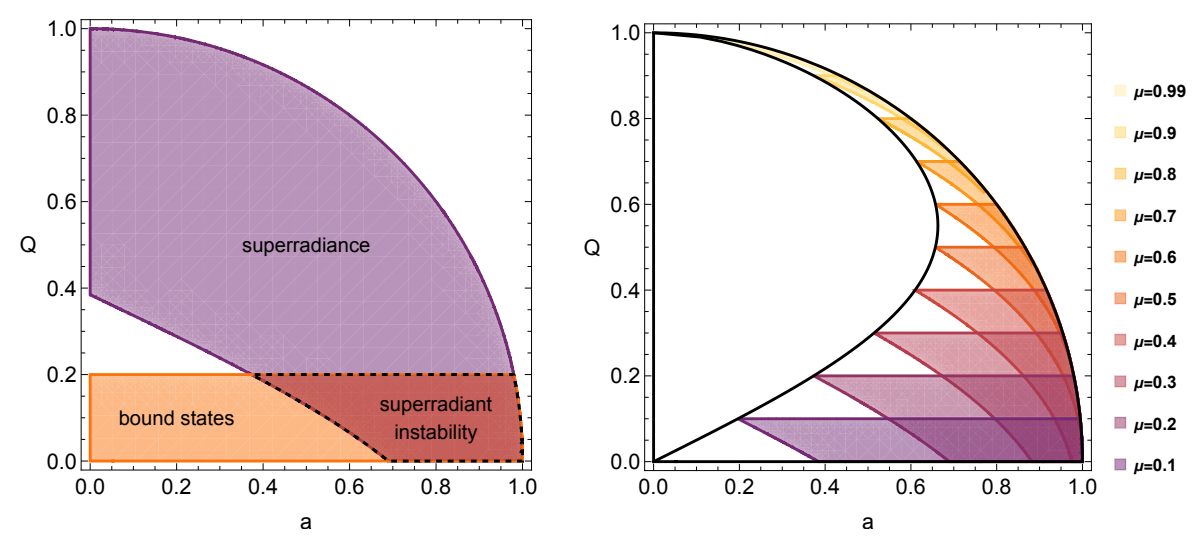


Figure 3: Plots of the superradiant region for (a) Kerr, (b) Reissner-Nordström, (c) Kerr-Newman as a function of a for various values of Q, and (d) Kerr-Newman as a function of Q for various values of a.

region $Q < \mu$. The superradiant region is simply given by (4.13). For example, these regions are shown in fig. 4a for the value $\mu = 0.2$. We are interested in the overlap between these two regions, of course, which is the region where the black hole may develop a superradiant instability. The region of superradiant instability is shown in fig. 4b for various values of μ . The boundary of the union of the superradiant intability regions for all values of μ from 0 to 1 is the solid black curve in fig. 4b and is given by setting $\mu = Q$ in (4.13) and solving for a:

$$a > \frac{Q(1 - Q^2 + \sqrt{(1 - Q^2)(1 + Q^4)})}{1 + Q^2}.$$
(4.14)



- (a) The superradiance region, quasibound state region, and their overlap for $\mu = 0.2$.
- (b) Superradiant instability regions for different values of scalar field mass μ .

Figure 4: Regions of superradiant instability with M = 1, q = 1, m = 1, N = 0.

Since we must also satisfy the condition $a^2 + Q^2 \le 1$, the region shrinks down to two points in the RN limit: Q = 0 and Q = 1. This is consistent with the well-known fact that Reissner-Nordström is stable against superradiance [39–41].

The plot also confirms that, for very small values of the scalar field mass parameter μ , the region of superradiant instability is confined to equally small values of the black hole charge Q. At values of μ appropriate for the QCD axion, we would essentially be confined to Kerr. However, if we were to entertain models with much larger values of μ , then we can see that a significant region opens up with considerable black hole charge. In fact, the extent of the superradiant instability region along the Kerr axis diminishes as μ increases and even vanishes for $\mu > 0.5$. Thus, above this value of the scalar field mass, we would only encounter superradiant instability for a Kerr-Newman black hole with some nonzero charge. As we continue to increase the scalar field mass, the black hole would have to become more charged and closer to extremal in order to potentially be unstable to superradiance.

5. Scalar Field Growth Rate

For the instability to occur effectively, the scalar field mode must grow over time. Therefore, we impose the condition

$$\operatorname{Im} \omega > 0. \tag{5.1}$$

Again, we expand (4.7) around $\mu = \mu_0$ and solve for ω to lowest order in $\mu - \mu_0$ which gives the following result for the imaginary part,

$$\operatorname{Im} \omega = \frac{1}{2} \left(\frac{D^2 M^2 \mu_0 [am + (Q^2 - M^2)\mu_0]}{(\overline{N}D)^2 + [am + (Q^2 - M^2)\mu_0]^2} \right) (\mu - \mu_0)^2.$$
 (5.2)

This analysis also demonstrates that $\operatorname{Re}\left[\sqrt{\mu^2-\omega^2}\right]$ and $\operatorname{Im}\omega$ both go to zero at the point $\mu=\mu_0=qQ/M$. However, $\operatorname{Im}\omega\propto(\mu-\mu_0)^2$, with a positive coefficient, and so $\operatorname{Im}\omega>0$ both to the right and to the left of $\mu=\mu_0$. In other words, there is potential for superradiant instability even in the region $\mu<\mu_0$, but the lack of quasibound states in that region prevents the instability from developing. In the region $\mu>\mu_0$, however, there are quasibound states and so superradiant instability does occur, up to some cut-off μ where $\operatorname{Im}\omega$ once again goes to zero and switches sign from positive to negative. These results are shown in fig. 5.

We can determine the point where Im ω becomes negative perturbatively in the smallness of $\mu - \omega$. To first order (i.e., keeping only up to linear order in $\mu - \omega$), this point is

$$\mu_1^{(1)} = \frac{am + qQ}{2M^2 - Q^2}. (5.3)$$

To second order (i.e., keeping up to quadratic order in $\mu - \omega$), this point is found to be

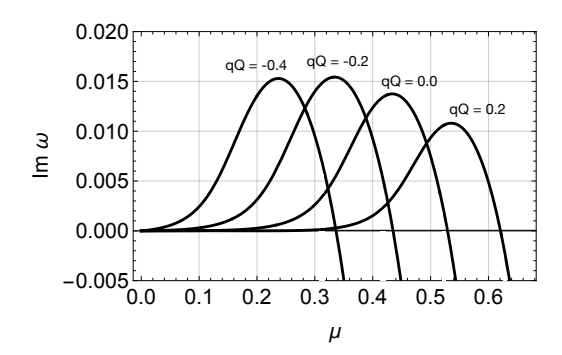
$$\mu_1^{(2)} = \mu_1^{(1)} \left(1 + \frac{[am + \mu_0(Q^2 - M^2)]^2 M^2}{2\overline{N}^2 (Q^2 - 2M^2)^2 + [am + \mu_0(Q^2 - M^2)][3am - \mu_0(Q^2 - 5M^2)]M^2} \right). (5.4)$$

Let us compare these results with Furuhashi and Nambu [37] by producing a plot of qQ versus μM showing the region where there are no quasibound states, the region where there is no superradiant instability, and the shaded region where there are both quasibound states and superradiance. This is done numerically in fig. 3 of [37], but we can plot the boundary by eye since it is approximately linear. On the other hand, our expressions, $\mu_1^{(1)}$ to first order and $\mu_1^{(2)}$ to second order, can be plotted exactly. We include several data points of the exact result, which proves to be well approximated by our second-order $\mu_1^{(2)}$ analytic result. These results are shown in fig. 6.

5.1. The Analytics vs. Numerics Discrepancy

In [29], the authors claim that their plot of $\text{Im }\omega$ in their fig. 3 shows that the resonant frequencies "have a behavior which is similar to the results presented" in fig. 6 of [37]. We have three qualifications to this statement:

- 1. The statement compares apples to oranges: the parameters in fig. 3 of [29] are m = -1, q = 1, a = 0.99M, and Q = 0.01M, whereas those in fig. 6 of [37] are m = 1, a = 0.98M, and Q = 0.01M and the parameter q is the one being tuned.
- 2. Fig. 3 in [29] does not depict the behavior of $\text{Im }\omega$ where it vanishes near the point $\mu = \mu_0 = qQ/M$. This is because $\mu_0 = 0.01$ in this case and one would need to zoom in significantly towards the origin of these plots to show this. The corresponding (dashed) curve in fig. 6 of [37] uses q = 0 instead and so $\mu_0 = 0$ in this case.



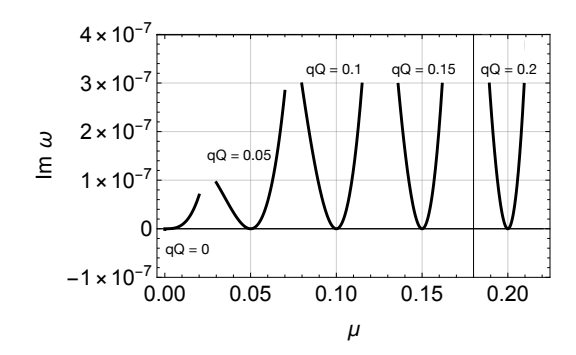


Figure 5: Plots of $\operatorname{Im} \omega$ vs. μ with a=0.98M, Q=0.01M, M=1, m=1, N=0 and q as the tuning parameter. The left figure shows the points where $\operatorname{Im} \omega$ turns negative for different values of qQ. The right figure shows portions of the plots zoomed into the region near $\mu=\mu_0=qQ/M$ for several positive values of qQ.

3. Most importantly, there is a *quantative* difference between where the numerics of Furuhashi and Nambu place the boundary line beyond which superradiance stops and where our analytic analysis of the VBK resonance equation to first- and second-order places this boundary line, as can be seen in fig. 6.

This quantitative tension between the exact analytic results of [29] and the numerical results of [37] arises for the following reason. The radial equation that Furuhashi and Nambu analyze numerically contains an effective potential that takes the form of the one that comes from the hydrogenic approximation. By this, we mean that they take the separation constant that comes from the method of separation of variables to have the form $\lambda = \ell(\ell+1)$, where ℓ is an angular momentum quantum number whose relation to the "magnetic" quantum number m is the usual one that is appropriate for the hydrogen atom: $\ell = 0, 1, 2, \ldots$ and $-\ell \le m \le \ell$. However, the polar-angular equation in the case of a Klein-Gordon field in a Kerr-Newman background reads

$$\frac{1}{\sin\theta} \frac{d}{d\theta} \left(\sin\theta \frac{dP}{d\theta} \right) + \left(\lambda - \frac{m^2}{\sin^2\theta} + a^2(\mu^2 - \omega^2) \sin^2\theta \right) P = 0, \tag{5.5}$$

where λ is the separation constant. For the hydrogen atom, the term $a^2(\mu^2 - \omega^2)\sin^2\theta$ is absent, the solutions take the form of associated Legendre functions, and the separation constant takes the familiar form $\lambda = \ell(\ell+1)$. In making their numerical plots, Furuhashi and Nambu take $\ell = 1$ (and m = 1), for example. These, however, are not the actual solutions of the angular equation of interest (5.5). The degree to which they are good approximate solutions is the degree to which $\omega \approx \mu$ and/or $\mu M, \omega M \ll 1$. From fig. 6, it is clear that the boundary line where superradiance stops occurs at values of μM that are not $\ll 1$. Furthermore, our first-order (5.3) and second-order (5.4) analytic boundary lines plotted in

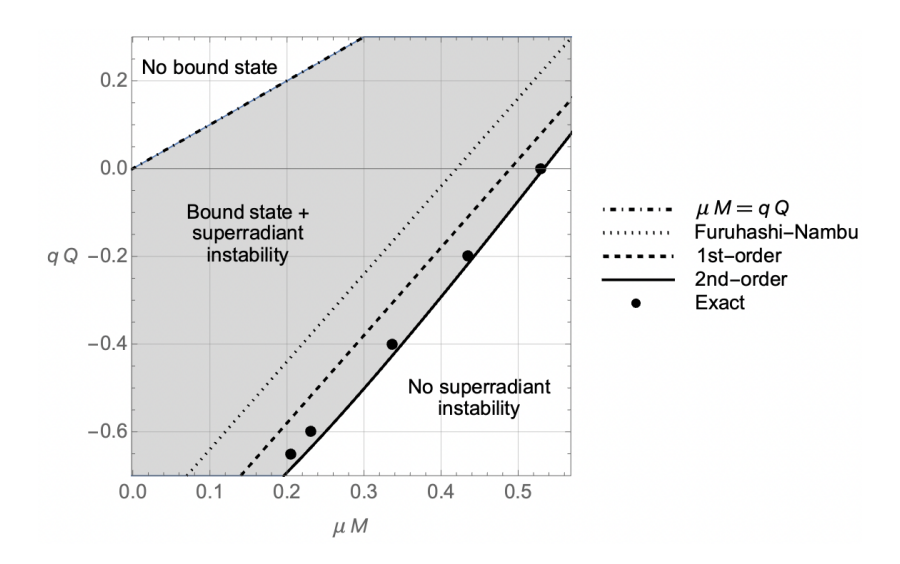


Figure 6: Plot showing the regions in the μM and qQ plane (parameter values a=0.98M, Q=0.01M, m=1) where there are quasibound states and superradiance (shaded gray). The dotdashed line corresponds to $\mu M=qQ$ and is the boundary of the region with no quasibound states. The boundary of the region with no superradiance is the dotted line according to the numerical analysis of Furuhashi and Nambu [37], the dashed line according to our first-order analytic result (5.3), and the solid line according to our second-order analytic result (5.4). The circle points are exact results from solving the resonance equation of Vieira, Bezerra, and Muniz [29].

fig. 6 are first- and second-order precisely in the difference $\mu - \omega$. In this respect, the result of Furuhashi and Nambu may be thought of as the "zeroth-order" counterpart to our first-and second-order results.

It is a remarkable fact that the characteristic resonance equation for ω is independent of the separation constant λ . The authors of [29] point this out explicitly. It is what allows them to write down the resonance equation without having to determine the allowed values of the separation constant by solving the angular equation first. Therefore, the numerics may get different boundary lines for different values of ℓ and they almost certainly will. Nevertheless, the true boundary line, as well as our first- and second-order approximations of it, do not depend on λ at all and, therefore, do not depend on how well λ is approximated by the form $\lambda = \ell(\ell+1)$. The dependence on ℓ is instead *implicit* through the so-called "overtone number" N (or $\overline{N} = N+1$) in that, at least in the hydrogenic limit, N would be related to the principal quantum number n and the angular momentum quantum number ℓ via $N = n + \ell$.

6. Conclusion and Outlook

In this paper we used the Vieira-Bezerra-Kokkotas (VBK) method to specify the regions of black hole superradiant instability as a function of the black hole parameters (spin a and

charge Q) and scalar field mass μ . This exact method allows us to obtain analytic control over the parameter space of quasibound and superradiant modes without resorting to the hydrogenic approximation or numerics.

We solved for the quasibound states and the superradiant states and plotted their respective regions in the parameter space. The overlap regions determine the parameters in which superradiant instability will occur. We found that for very small values of μ , we have superradiant instability for black holes that have a very small charge $Q < \mu$ (in units of M=1 and q=1). Likewise, we also determined that for black holes that have very small spin values a, the overlap region vanishes. This is especially apparent if we take greater values of μ . To compensate, the black hole must then be highly charged and closer to the extremal case in order to potentially be unstable to superradiance. Essentially,

- For small values of the scalar field mass $\mu M \ll 1$, black holes that are closer to being "Kerr-like" than "RN-like" are more susceptible to superradiant instability.
- For large values of the scalar field mass $\mu M \lesssim 1$, Kerr-Newman black holes that are highly charged, have non-zero spin a, and are close to extremal are the ones which are susceptible to superradiant instability.
- For in-between values of μ , refer to fig. 4b.

Thus, we have provided a unified and exact characterization of the region of superradiant instability of Kerr-Newman black holes in the presence of a massive real scalar field. These results extend the standard results in the literature, which were mostly confined to small scalar field mass $\mu M \ll 1$ or Kerr black holes.

We also performed an expansion of the characteristic resonance equation (3.9) near the point $\mu = \mu_0$, which is the point where $\omega = \mu$. The parameter $\text{Re}\left[\sqrt{\mu^2 - \omega^2}\right]$ is positive for $\mu > \mu_0$, meaning that the scalar field decays towards infinite radial distance from the black hole and is thus quasibound, and is negative for $\mu < \mu_0$. This tells us that quasibound states will only form for scalar fields with $\mu > \mu_0$. We also checked the region around μ_0 and determined if these parameters satisfy $\text{Im }\omega > 0$, thus allowing the scalar field to grow exponentially over time. We discovered that in the regions $\mu < \mu_0$ and $\mu > \mu_0$, $\text{Im }\omega > 0$, hence, in both regions the scalar field mode can grow. However, since the region $\mu < \mu_0$ does not satisfy the quasibound state condition, black hole instability does not develop there. Thus, only in the region $\mu > \mu_0$ do we expect to have instabilities due to superradiance.

We derived analytic expressions for the boundary line beyond which Im ω becomes negative. Beyond this line, the scalar field no longer grows over time preventing the development of a superradiant instability. These expressions are $\mu_1^{(1)}$ (5.3) and $\mu_1^{(2)}$ (5.4), to linear and quadratic order in $\mu - \omega$, respectively. This is compared with several data points of the exact result derived from the plot of the exact solution for Im ω as a function of μ and fig. 6 shows good agreement between the exact result and the second-order result $\mu_1^{(2)}$. There is a clear difference between these exact results and the numerical results of Furuhashi and Nambu [37]. We attribute the discrepancy to the approximation $\omega \approx \mu$ used in the numerical analysis and

therefore our first- and second-order results can be thought of as corrections to the numerical. Furthermore, the exact VBK method now allows us to pinpoint the *exact* location of the boundary beyond any approximations.

As possible extensions of this work, it would be interesting to study other black hole spacetimes outside the Kerr-Newman family, such as Kerr-Newman-Kasuya (dyonic) black holes. It would also be interested to study spacetimes with different boundary or asymptotic conditions (e.g., AdS). We can also study fields with higher spin (e.g., massive vector fields). There is also opportunities in further numerical analyses including of the aforementioned systems and potentially including backreaction. Finally, it would be interesting to study systems of astrophysical interest, including binary systems, and making contact with gravitational waves.

Acknowledgments

K.T.G. would like to acknowledge financial support from the National Institute of Physics, University of the Philippines, Diliman Research Grant Project "Superradiance and Quasi-Bound States in the Parameter Space of the Kerr-Newman Black Hole."

References

- P. S. Cole, G. Bertone, A. Coogan, D. Gaggero, T. Karydas, B. J. Kavanagh et al., Distinguishing environmental effects on binary black hole gravitational waveforms, Nature Astron. 7 (2023) 943–950, [2211.01362].
- [2] V. Cardoso, K. Destounis, F. Duque, R. P. Macedo and A. Maselli, *Black holes in galaxies: Environmental impact on gravitational-wave generation and propagation*, *Phys. Rev. D* **105** (2022) L061501, [2109.00005].
- [3] P. Sarmah, H. Verma, K. Cheung and J. Silk, Effects of superradiance in active galactic nuclei, Mon. Not. Roy. Astron. Soc. 538 (2025) 943–962, [2404.09955].
- [4] A. Lupsasca, D. R. Mayerson, B. Ripperda and S. Staelens, A Beginner's Guide to Black Hole Imaging and Associated Tests of General Relativity, in Recent Progress on Gravity Tests. Challenges and Future Perspectives (C. Bambi and A. Cardenas-Avendano, eds.), pp. 183–237. Springer, 2024. 2402.01290.
- [5] M. S. Oei, M. J. Hardcastle, R. Timmerman et al., *Black hole jets on the scale of the cosmic web*, *Nature* **633** (2024) 537–541, [2411.08630].
- [6] R. Brito, Black holes as laboratories: searching for ultralight fields, Gen. Rel. Grav. 57 (2025) 42.
- [7] D. Blas, Black hole superradiance to search for new particles, in 33rd Rencontres de Blois: Exploring the Dark Universe, 11, 2022, 2211.02067.
- [8] L. Hui, Y. T. A. Law, L. Santoni, G. Sun, G. M. Tomaselli and E. Trincherini, *Black hole superradiance with dark matter accretion*, *Phys. Rev. D* **107** (2023) 104018, [2208.06408].

- [9] R. Brito, V. Cardoso and P. Pani, Superradiance: New Frontiers in Black Hole Physics, Lect. Notes Phys. 906 (2015) pp.1–237, [1501.06570].
- [10] J. D. Bekenstein and M. Schiffer, The Many faces of superradiance, Phys. Rev. D 58 (1998) 064014, [gr-qc/9803033].
- [11] D. M. Lukin, M. A. Guidry, J. Yang, M. Ghezellou, S. D. Mishra, H. Abe et al., Optical superradiance of a pair of color centers in an integrated silicon-carbide-on-insulator microresonator, 2202.04845.
- [12] E. Sierra, S. J. Masson and A. Asenjo-Garcia, Dicke Superradiance in Ordered Lattices: Dimensionality Matters, Phys. Rev. Res. 4 (2022) 023207, [2110.08380].
- [13] P. Stránský and P. Cejnar, Superradiance in finite quantum systems randomly coupled to continuum, Phys. Rev. E 100 (2019) 042119, [1907.11576].
- [14] H. Eleuch and I. Rotter, Open quantum systems and Dicke superradiance, Eur. Phys. J. D 68 (2014) 74, [1305.2762].
- [15] V. Cardoso, O. J. C. Dias, J. P. S. Lemos and S. Yoshida, *The Black hole bomb and superradiant instabilities*, *Phys. Rev. D* **70** (2004) 044039, [hep-th/0404096].
- [16] W. H. Press and S. A. Teukolsky, Floating orbits, superradiant scattering and the black-hole bomb, Nature 238 (1972) 211–212.
- [17] D. Baumann, H. S. Chia, J. Stout and L. ter Haar, The Spectra of Gravitational Atoms, JCAP 12 (2019) 006, [1908.10370].
- [18] O. J. C. Dias, G. Lingetti, P. Pani and J. E. Santos, Black hole superradiant instability for massive spin-2 fields, Phys. Rev. D 108 (2023) L041502, [2304.01265].
- [19] G. M. Tomaselli, T. F. M. Spieksma and G. Bertone, Legacy of Boson Clouds on Black Hole Binaries, Phys. Rev. Lett. 133 (2024) 121402, [2407.12908].
- [20] G. M. Tomaselli, T. F. M. Spieksma and G. Bertone, Resonant history of gravitational atoms in black hole binaries, Phys. Rev. D 110 (2024) 064048, [2403.03147].
- [21] M. Baryakhtar, M. Galanis, R. Lasenby and O. Simon, *Black hole superradiance of self-interacting scalar fields, Phys. Rev. D* **103** (2021) 095019, [2011.11646].
- [22] M. Baryakhtar, R. Lasenby and M. Teo, Black Hole Superradiance Signatures of Ultralight Vectors, Phys. Rev. D 96 (2017) 035019, [1704.05081].
- [23] R. Vicente, V. Cardoso and J. C. Lopes, Penrose process, superradiance, and ergoregion instabilities, Phys. Rev. D 97 (2018) 084032, [1803.08060].
- [24] A. A. Starobinskii, Amplification of waves during reflection from a rotating "black hole", Sov. Phys. JETP 37 (1973) 28–32.
- [25] S. Detweiler, Klein-gordon equation and rotating black holes, Phys. Rev. D 22 (Nov, 1980) 2323–2326.
- [26] A. Arvanitaki, M. Baryakhtar and X. Huang, Discovering the QCD Axion with Black Holes and Gravitational Waves, Phys. Rev. D 91 (2015) 084011, [1411.2263].
- [27] D. Baumann, G. Bertone, J. Stout and G. M. Tomaselli, Ionization of gravitational atoms, Phys. Rev. D 105 (2022) 115036, [2112.14777].

- [28] H. S. Vieira and K. D. Kokkotas, Quasibound states of Schwarzschild acoustic black holes, Phys. Rev. D 104 (2021) 024035, [2104.03938].
- [29] H. S. Vieira, V. B. Bezerra and C. R. Muniz, Instability of the charged massive scalar field on the Kerr-Newman black hole spacetime, Eur. Phys. J. C 82 (2022) 932, [2107.02562].
- [30] S. R. Dolan, Instability of the massive Klein-Gordon field on the Kerr spacetime, Phys. Rev. D 76 (2007) 084001, [0705.2880].
- [31] W. E. East and F. Pretorius, Superradiant Instability and Backreaction of Massive Vector Fields around Kerr Black Holes, Phys. Rev. Lett. 119 (2017) 041101, [1704.04791].
- [32] A. Arvanitaki and S. Dubovsky, Exploring the String Axiverse with Precision Black Hole Physics, Phys. Rev. D 83 (2011) 044026, [1004.3558].
- [33] H. Yoshino and H. Kodama, Bosenova collapse of axion cloud around a rotating black hole, Prog. Theor. Phys. 128 (2012) 153–190, [1203.5070].
- [34] M. Baryakhtar, M. Galanis, R. Lasenby and O. Simon, *Black hole superradiance of self-interacting scalar fields, Phys. Rev. D* **103** (2021) 095019, [2011.11646].
- [35] N. Xie and F. P. Huang, Self-interaction effects on the Kerr black hole superradiance and their observational implications, Phys. Rev. D 112 (2025) 055028, [2503.10347].
- [36] Y. S. Myung, Conditions for superradiant instability of the Kerr-Newman black holes, Phys. Rev. D 105 (2022) 124015, [2204.06750].
- [37] H. Furuhashi and Y. Nambu, Instability of massive scalar fields in Kerr-Newman space-time, Prog. Theor. Phys. 112 (2004) 983–995, [gr-qc/0402037].
- [38] T. Adamo and E. T. Newman, The Kerr-Newman metric: A Review, Scholarpedia 9 (2014) 31791, [1410.6626].
- [39] V. Moncrief, Stability of Reissner-Nordström black holes, Phys. Rev. D 10 (1974) 1057–1059.
- [40] S. Hod, No-bomb theorem for charged Reissner-Nordström black holes, Phys Lett B 718 (2013) 1489–1492, [1304.6474].
- [41] S. Hod, Stability of highly-charged Reissner-Nordström black holes to charged scalar perturbations, Phys. Rev. D **91** (2015) 044047, [1504.00009].